Physical modeling III : acquiring modeled data for VVAZ/AVAZ analysis

Joe Wong, Faranak Mahmoudian, Eric Gallant, and Gary Margrave

ABSTRACT

CREWES has initiated a physical modeling project focused on acquiring seismic data suitable for VVAZ and AVAZ analysis. We fabricated three solid slabs with anisotropic properties to be used in this project. Two flat slabs simulating media with orthorhombic anisotropy were fabricated by joining sections of phenolic LE material. The first slab was constructed to approximate a homogeneous layer. The second slab was constructed to have two homogeneous sections, but with their axes of maximum horizontal velocity at right angles to each other. A third slab with 3D heterogeneity was constructed by embedding pucks of various diameters, cut from orthorhombic phenolic material, in an isotropic acrylic plastic slab. The three slabs are simple geometrically, but when used in combination with other isotropic slabs and targets of other shapes, we can set up models of surprising variety and complexity. Using the University of Calgary Seismic Physical Modeling Facility, we have recorded many SEG-Y files containing 2D seismic data targeted toward AVAZ/VVAZ investigations. In this report, we describe some of the 2D surveys, and present examples of raw and analyzed data.

INTRODUCTION

The University of Calgary Seismic Physical Modeling System (Wong et al., 2009) enables us to conduct seismic surveys over physical models that are scaled down versions of idealized geological targets. Dimensions are scaled so that 1 mm in the physical model represents 10 m in the real world, and frequencies are scaled so that 1 MHz in the physical model represents 100 Hz in the real world. Piezoelectric transducers are used as generators and detectors of acoustic and/or elastic waves.

Seismic physical modeling can provide data that bridge the gap between data calculated from numerical models and data recorded in real-world surveys. Algorithms that produce numerical seismic results often need to be validated by being checked against controlled experimental observations. Real-world surveys often produce data that are difficult to understand and that cannot be simulated numerically. For both situations, scale-model measurements often provide valuable insights and lead either to required adjustments to computer codes, or to rational explanations of field observations.

In the seismic industry, VVAZ and AVAZ effects are phenomena receiving growing attention as practitioners attempt to provide more accurate structural images in anisotropic media. They also wish to increase the value of seismic data by relating VVAZ/AVAZ effects to fracture density and orientation. CREWES has undertaken a project to produce scale-model seismic data for anisotropic structures that are suitable for VVAZ and AVAZ analysis. By analyzing such data, we hope to develop techniques that improve the fidelity of final migrated images for anisotropic geological structures. We also hope to identify (perhaps) more diagnostic VVAZ and AVAZ attributes suitable for

3D visualization. The physically-modeled data recorded on SEG-Y files will be made available to our industrial sponsors upon request.

CONSTRUCTING MODELS WITH ORTHORHOMBIC ANISOTROPY

Three anisotropic solids (shown on Figure 1) were constructed to be used for the VVAZ/AVAZ measurements.

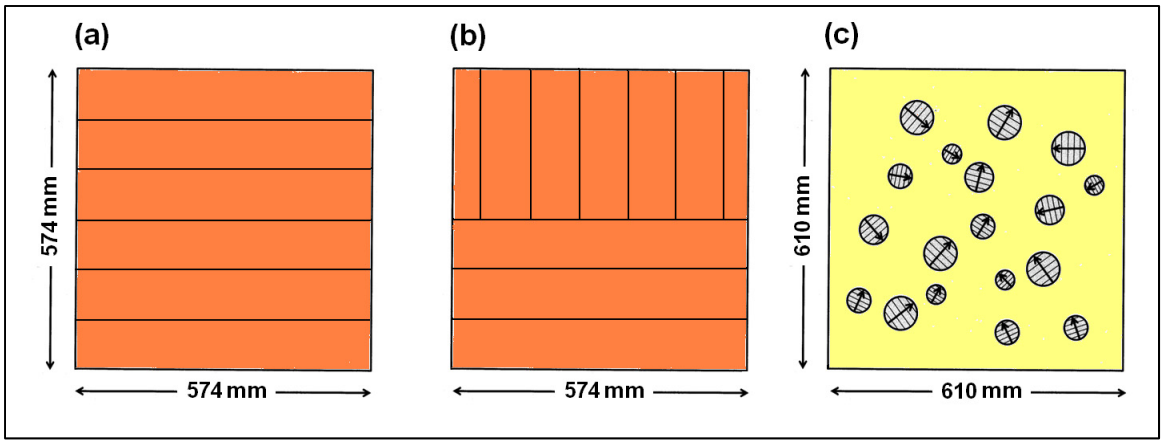

FIG. 1. Plan views of three solid slabs fabricated from phenolic and acrylic plastic materials. The lines on Figures 1a and 1b indicate seams where sections of phenolic material are joined. On Figure 1c, the yellow material is isotropic acrylic plastic, the circles represent orthorhombic phenolic, with arrows pointing in the direction of maximum P-wave velocity (3550 m/s).

The first anisotropic solid (Figure 1a) is a slab with orthorhombic anisotropy. It was fabricated by cutting sections of phenolic material and gluing them together so they formed a single slab 574 mm by 574 mm by 69.2 mm thick. The sections of phenolic were arranged so that the slab as whole has P-wave velocities of about 3550 m/s parallel to the seams (x-direction), about 2950 m/s perpendicular to the seams (y-direction), and about 3400 m/s in the thickness direction (z-direction). These values are within 3% of the values given on Table 2 of Mahmoudian et al. (2010).

The second anisotropic solid is a slab measuring 574 mm by 574 mm by 69.2 mm thick that consists of two orthorhombic sections with their directions of maximum P-wave velocity perpendicular to each other. It was fabricated by arranging and gluing phenolic sections as shown on Figure 1b. The velocities in the x and y directions are again approximately 3550 m/s and 2950 m/s, and 3400 m/ in the thickness or z direction.

The third anisotropic solid (Figure 1c) is an acrylic plastic slab (610 mm by 610 mm by 50.8 mm thick) with a number of embedded phenolic “pucks”. The pucks have different diameters ranging from 40 mm to 70 mm, but all are 25.4 mm thick. The top surfaces of the pucks are flush with the top surface of the acrylic slab. The acrylic plastic is isotropic, but the pucks have orthorhombic anisotropy. The maximum and minimum velocities of the pucks in the horizontal plane are again 3550 m/s and 2950 m/s. They are arranged so that their directions of maximum velocity are different (but documented).

Phenolic by itself when immersed in water will absorbed water. To prevent this, all the fabricated slabs were covered with a very thin coating of water-proof sealant.

ACQUISITION

A variety of velocity models can be set up by using these solids in combination with an isotropic acrylic slab. The anisotropic slabs can be immersed in a water-filled tank within the modeling space with different orientations of the principal velocity axes relative to the x and z axes of the modeling system. Placing one layer by itself in the water produces a two-layer velocity model. Placing an extra isotropic acrylic plastic slab over the anisotropic slab and immersing both slabs provide a three-layer model. A short cylindrical PVC target could be placed under the horizontal slabs for a model with added geometric complexity.

At the time of writing of this report, our scale model acquisition for VVAZ/AVAZ analysis has been done using only the homogeneous orthorhombic solid shown on Figure 1a. It is the simplest of the three fabricated slabs, and we investigate it first to learn best-practice acquisition techniques. As the project evolves, we will conduct 2D and 3D surveys over targets involving the more complicated inhomogeneous solids of Figures 1b and 1a. In the following sections of this report, we will present some of the data collected so far using the homogeneous slab.

Recording VVAZ data

To acquire data for VVAZ analysis, surveys were carried out with contact piezoelectric transducers on the solid surfaces of the homogeneous orthorhombic phenolic slab. One transducer (TX) acts as a source that generates ultrasonic vibrations in the solid medium. The second transducer (RX) acts as a receiver that detects the vibrations. We used V103 (P-type) and V153 (S-type) transducers from Olympus Corporation. V103 transducers will produce and detect vibrations primarily with particle motion in the vertical direction. V153 transducers, on the other hand, will produce and detect vibrations primarily with particle motion in a single preferred horizontal direction.

Signals recorded with V103 transducers as both source and detector primarily will be due to vertical P-wave motion. Signals recorded with V153 transducers as both source and detector primarily will be due to horizontal S-wave motion. Each V153 transducer can be rotated in the horizontal plane to produce or detect horizontal particle motion mainly in two orthogonal directions. If the source is a V103 transducer and the detector is a V153 transducer, measurements will simulate P-S land surveys. By using the appropriate combinations and orientations of transducers, scale-model measurements can simulate three-component seismic surveys on land.

Figure 2 shows two configurations of source and receiver placements on the surfaces of the orthorhombic slab: a top-surface configuration (Figure 2a), and a through-slab configuration (Figure2b). On Figure 2c, we indicate that survey lines can run at various azimuth angles φ to the x-axis of the acquisition coordinate system. For the measurements presented in this section, the seams of the homogeneous orthorhombic slab were aligned with the x-axis, and the thickness direction of the slab is along the z-axis.

The results of the data gathered for VVAZ were previously reported in detail by Mahmoudian et al. (2010). Here, we give a condensed version.

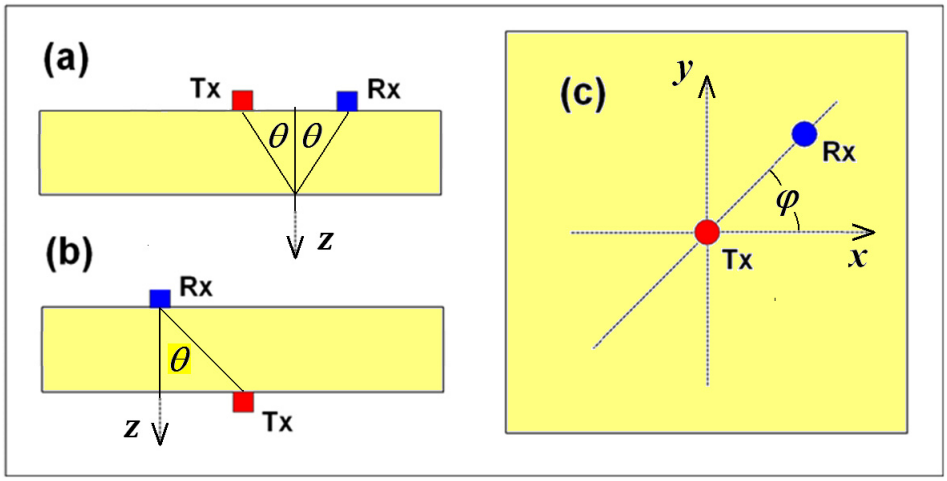

FIG. 2. Placement of source (TX) and receiver (RX) transducers on the solid slabs. (a) Surface configuration: TX fixed on top surface and Rx moving on top surface. (b) Through configuration: TX fixed on bottom surface and Rx moving on top surface. (c) Plan view of top surface with a line at azimuth φ along which Rx moves for both configurations.

Top Surface Measurements

Figure 3a shows 17 fixed-source end-on lines along various azimuths (φ = 0º, ±14º, ±27º, ±37º, ±45º, ±53º, ±63º, ±76º, ±90º) on the top surface of the homogeneous orthorhombic solid. Figure 3b displays an example gather of P-wave seismograms at φ = 14º. The blue line corresponds to the trajectory of first arrival times; its slope gives the velocity at this azimuth.

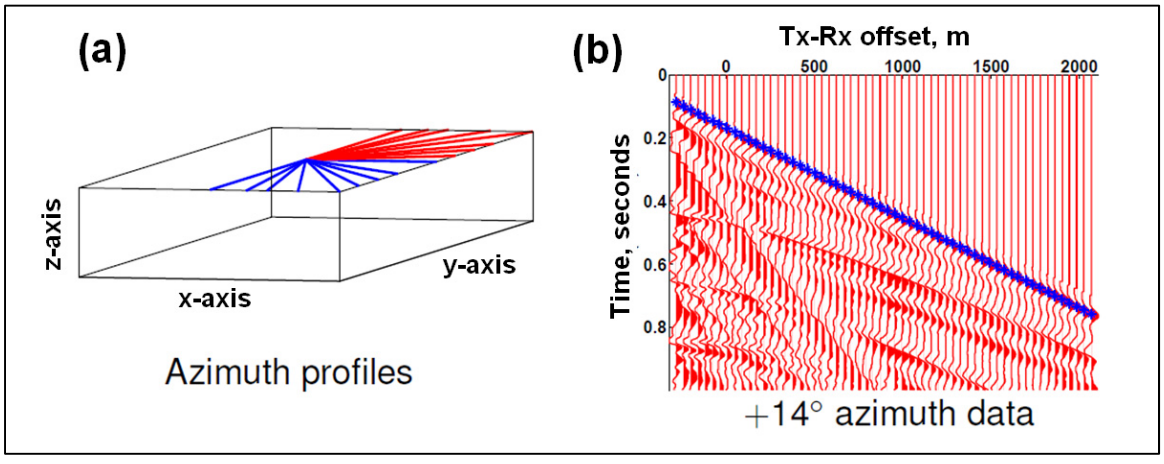

Figure 3: (a) Fixed-source survey lines at various azimuths on the top surface of the homogeneous orthorhombic solid; (b) an example gather of P-wave seismograms at φ = 14º.

In addition, P-P seismograms were recorded for two fixed-source split-spread profiles in the x and the y directions (Figures 4a and 4b). The traces are displayed on Figures 4c and 4d with manual time picks of the first arrivals plotted as small black crosses.

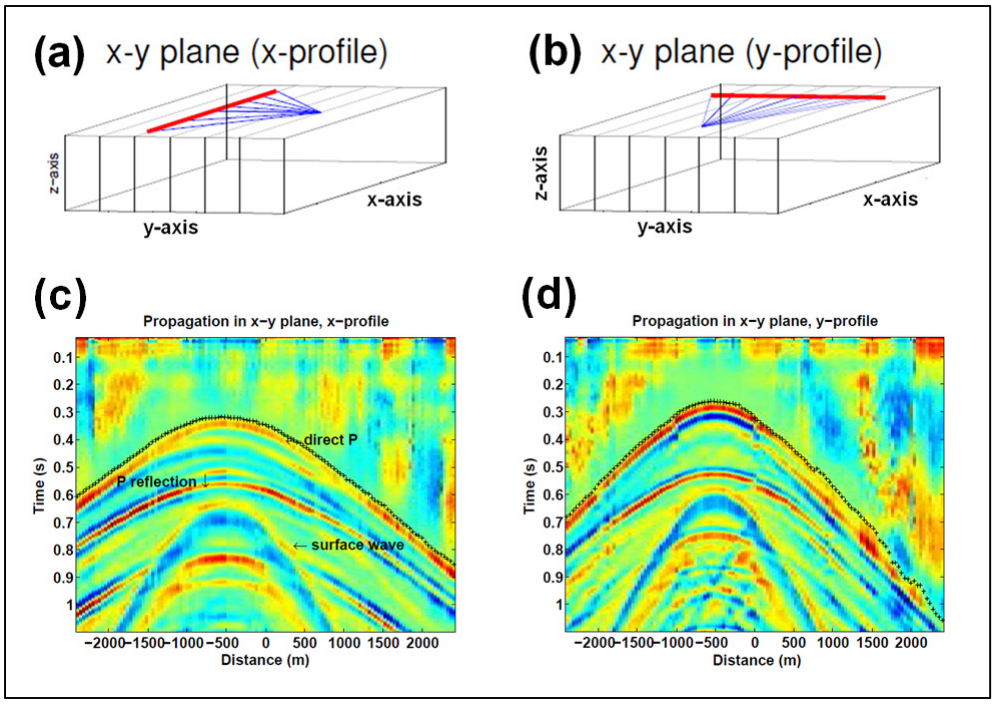

FIG. 4. Split-spread CSG surface profiles for Solid # 1, TX is offset from line by 100 m; (a) x-profile, parallel to x-axis; (b) y-profile, parallel to y-axis; (c) seismograms for x-profile; (d) seismograms for y-profile.

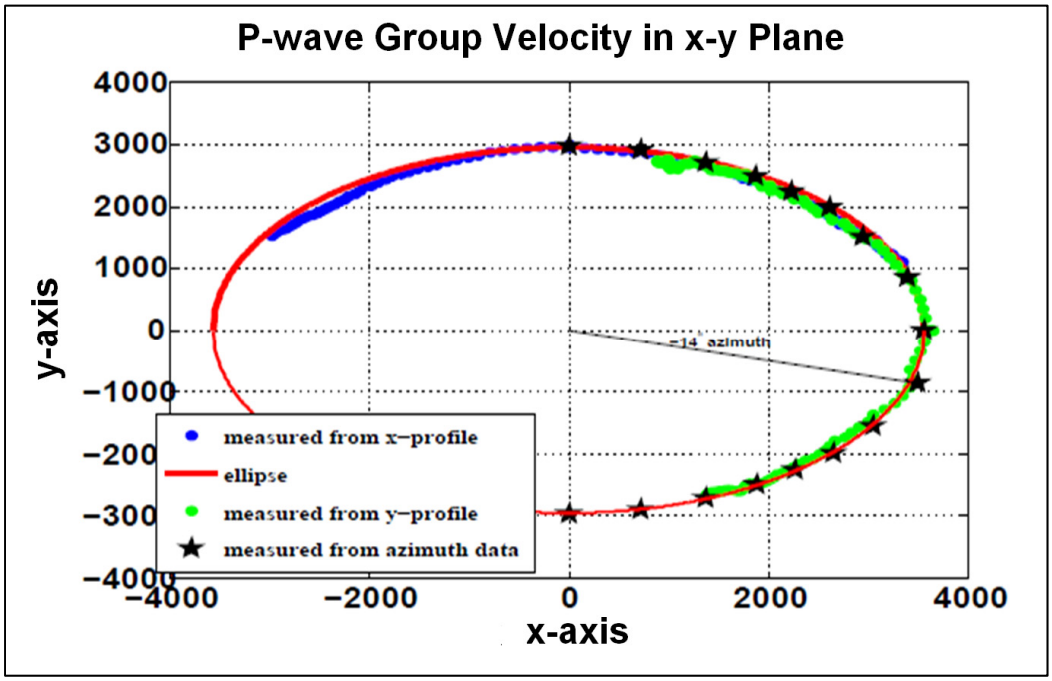

FIG 5. VVAZ in the x-y plane distilled from P-P measurements made on the top surface of the homogeneous orthorhombic slab. Velocity values have an estimated uncertainty of about ±2% due to time-picking errors and uncertainties in determining TX-RX separations.

First arrival times were picked for all the surface profiles. From the arrival times, qP group velocities can be calculated for various azimuths. Figure 5 is a summary plot of the VVAZ behaviour in the x-y plane. The observed group velocities for qP waves in the x-y plane fall on an elliptical pattern for our fabricated homogeneous orthorhombic slab.

Through Slab Measurements

P-P and S-S seismograms were also acquired through the homogeneous orthorhombic slab. Figure 6 is a schematic showing this acquisition geometry. The source transducer was fixed on the bottom surface of the slab. The receiver transducer moved along survey lines on the top surface at four azimuth angles (φ = 0º, ±45º, 90º). These measurements yield seismograms can be used to determine the qP and qS velocities in the x-z and y-z-planes of the orthorhombic solid.

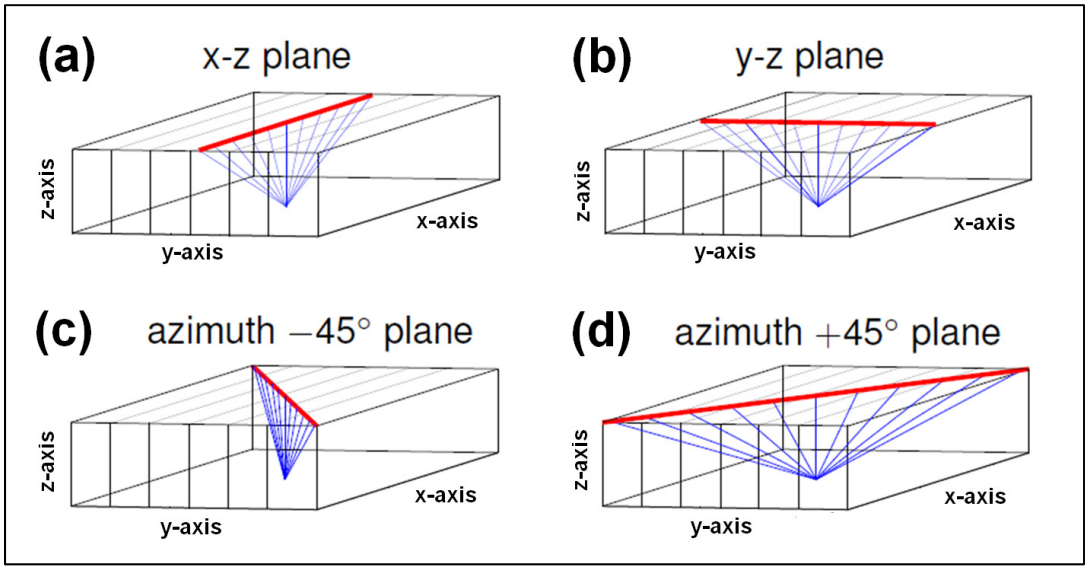

FIG. 6. Acquisition geometry for through-slab profiles. The receiver lines are plotted in red.

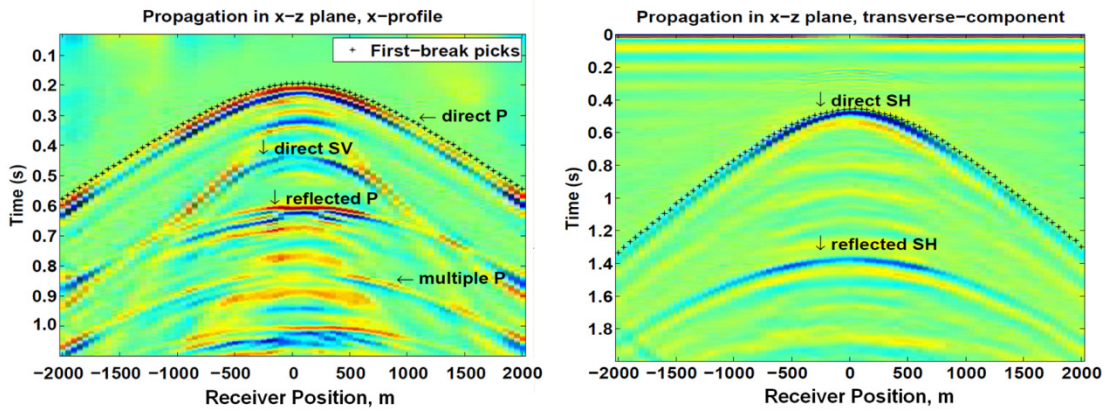

FIG. 7. Examples of through-slab seismograms recorded with P transducers (left), and with S transducers oriented transversely (right).

Examples of through-slab seismograms are plotted on Figure 7. Figure 7a displays a gather of traces recorded with two P-type transducers; Figure 7b shows a gather recorded with two S-type transducers with their response directions parallel to each other but normal to the profile direction. Such an orientation of response directions result in SH seismograms.

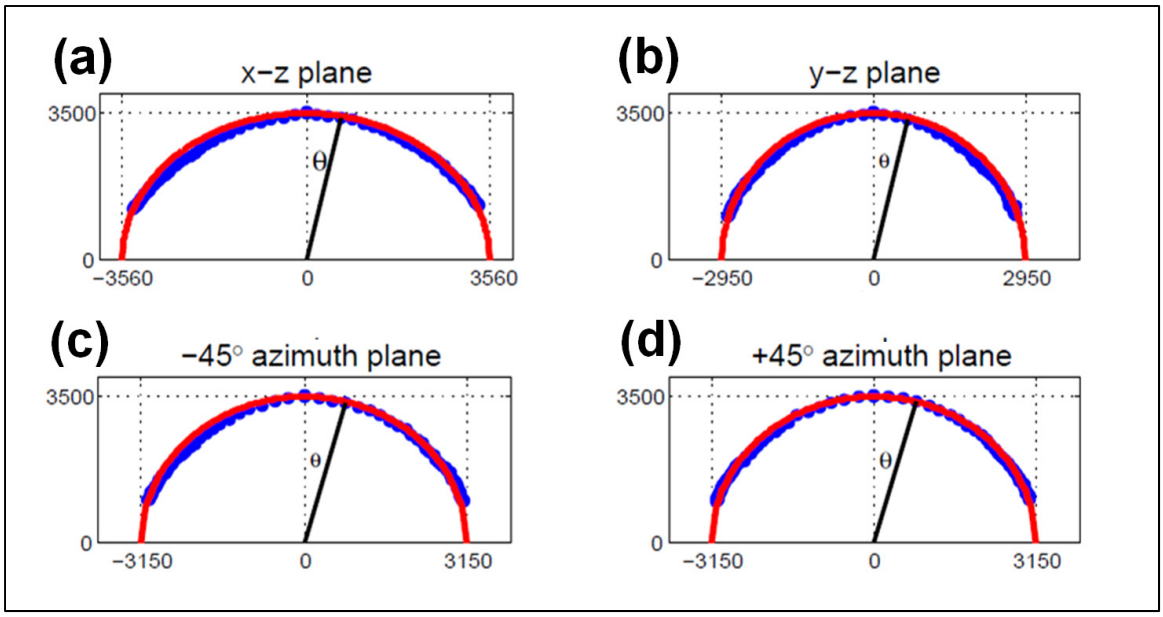

FIG. 8. AVAZ behaviour in vertical planes for qP waves in the orthorhombic solid. Velocity values have an estimated uncertainty of about ±3% due to time-picking errors and uncertainties in determining TX-RX separations.

VVAZ analysis using the seismograms recorded for the homogeneous orthorhombic solid have focused on the direct qP arrivals with a limited amount of analysis on the qS data (Mahmoudian et al., 2010). A complete treatment of the S-wave seismic gathers waits to be done (however, the data quality for the S waves is not as good as for the P-waves). It would also be interesting to investigate the VVAZ behaviour exhibited by the primary P-P reflections, which are quite strong and easy to identify.

Recording AVAZ data

Acquisition of data for AVAZ analysis was done using marine-type surveys over two different geometries involving the homogeneous orthorhombic solid (solid #1 of Figure 1a). The two model setups are shown on Figure 9. Figure 9a is a simple model that allows us to investigate AVAZ of reflection from the water-orthorhombic interface. Figure 9b is a more complicated model, since the AVAZ behaviour of the water-orthorhombic reflection is affected by the overlying isotropic acrylic layer.

Common midpoint (CMP) profiles were run along 16 azimuth angles (0º, ±14º, ±27º, ±37º, ±45º, ±57º, ±67º, ±76º, and 90º) relative to x-axis of the modeling system. For both geometries, the reflections from the top of the homogeneous orthorhombic layer were the primary interest. Piezopin transducers (30.48 mm long and 2.36 mm dia.) were used as the source (TX) and receiver for the surveys.

For each model setup on Figure 9, the seams of the orthorhombic solid (which are parallel to the direction of fastest P-wave velocity) were aligned with the x-axis of the modeling coordinate system. We acquired seismograms for CMP profiles along the 16 azimuth angles. Then, for each model setup, we rotated the solid slabs so that the direction of fastest P-wave velocity for the orthorhombic solid was about 35º CCW from the x-axis, and repeated the acquisition for the rotated models. The reason for doing this was to confirm that the AVAZ behaviour also rotated to be in correspondence with the new orientation of the orthorhombic symmetry axes.

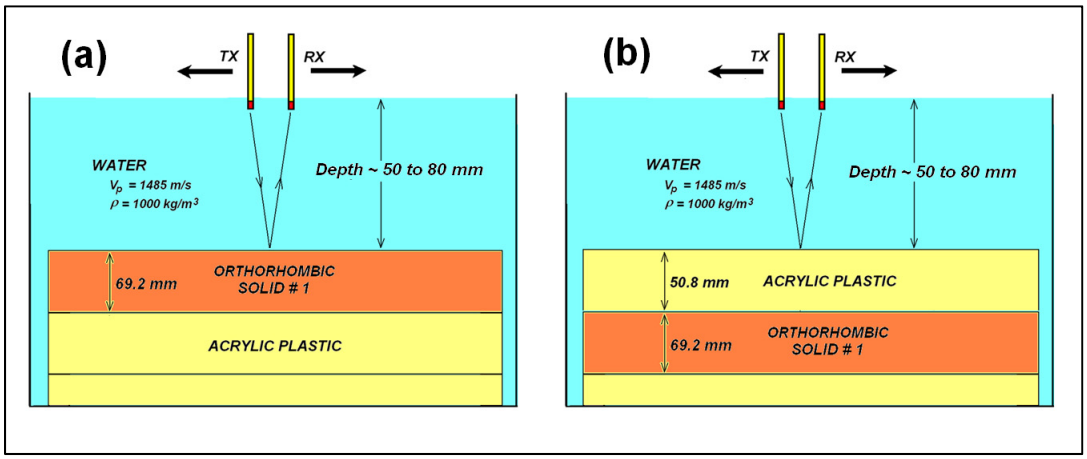

FIG. 9. Acquiring AVAZ data along CMP profiles over two models involving the homogeneous orthorhombic solid.

Examples of CMP gathers recorded over the unrotated model of Figure 9a are shown on Figure 10. AGC gain is necessary for the far-offset reflections to be visible. However, estimates of true event amplitudes must be made only on raw traces (band-pass-filtering is permissible, as long as it does not greatly affect trace amplitudes and as long as the pass-band is identical for all traces at all times).

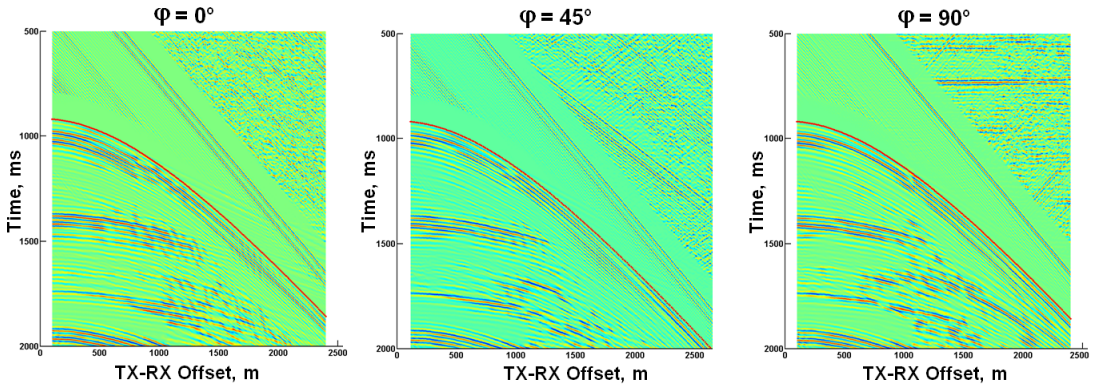

FIG. 10. CMP gathers with AGC gain for three azimuths over orthorhombic solid #1.

For the CMP gather at each azimuth, amplitudes of the reflections off the water-orthorhombic interface were estimated by the excursions from 0 of the first troughs in a short time window (length = 50 ms) following the picked reflection arrival times. The

estimated amplitudes were corrected for spherical divergence, and then scaled to be equal at near-zero offsets. The corrected and scaled amplitudes versus offset distance (i.e., AVO response) for the water-orthorhombic reflection are plotted on Figure 11. The differences in the AVO responses for azimuths of 0º, 45º, and 90º represent the AVAZ effect for the water-orthorhombic interface. We have noticed that the experimental AVAZ behaviour near the critical angle changes with depth to the reflecting interface. We speculate that this may be partly due to interference effects caused by the head-wave.

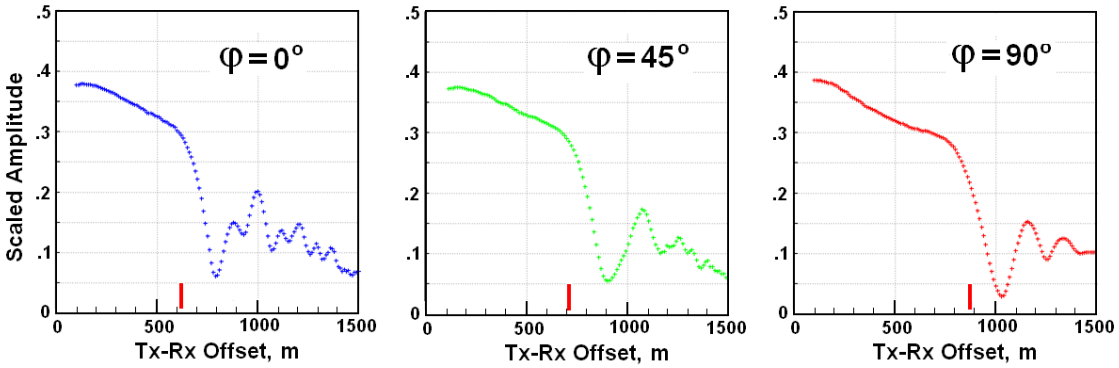

FIG. 11. AVO/AVAZ effect for reflection amplitudes from the water-orthorhombic interface of Figure 9a. The short vertical red line at each azimuth mark the critical distance.

The layers for the model shown on Figure 9b are displayed with more detail in the 3D view of Figure 12. Seismograms were acquired over this model along CMP profiles with azimuths of 0º, ±14º, ±27º, ±37º, ±45º, ±57º, ±67º, ±76º, and 90º. The intention was to gather data that could be used to investigate the AVAZ behaviour of the isotropic-orthorhombic reflection caused by the acrylic-phenolic interface.

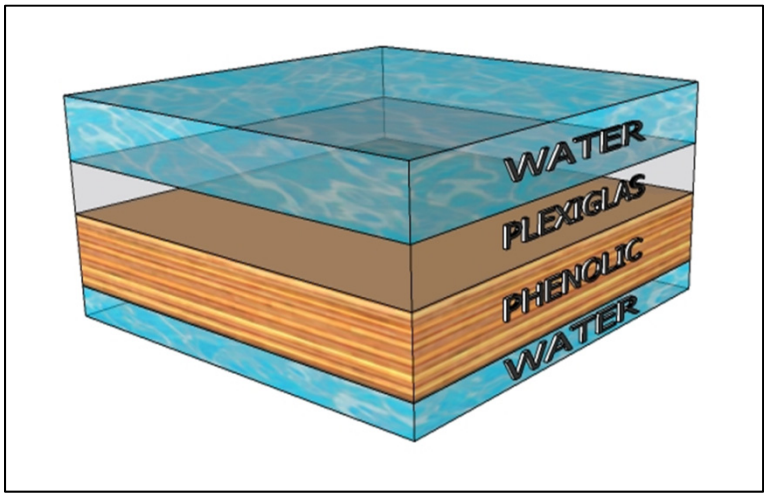

FIG. 12. 3D view of the model of Figure 9b shown with more detail.

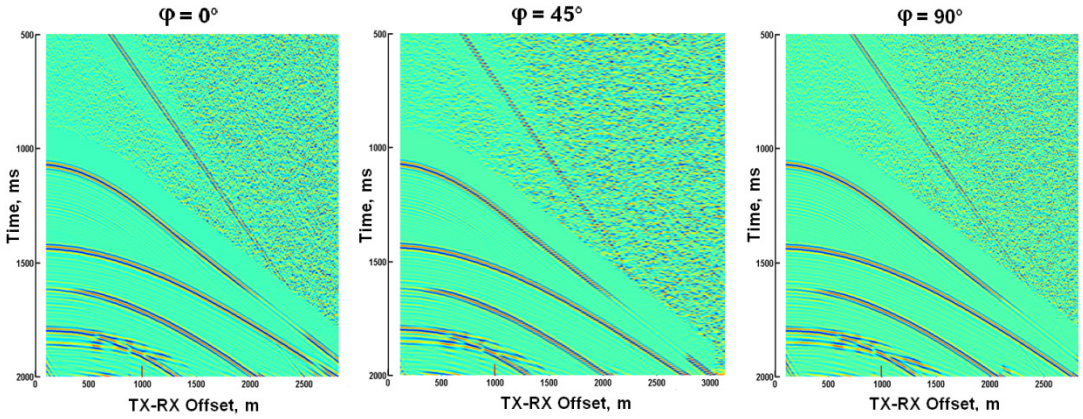

FIG 13. Three CMP gather over the model of Figure 12. Prominent reflections begin two-way times near 1040 ms, 1410 ms, and 1650 ms.

Examples of seismograms recorded over this layered model are plotted on Figure 13. It displays the CMP gathers with AGC gain for the azimuths φ = 0º, 45º, and 90º. On the plots, the reflection from the water-acrylic interface starts at about 1040 ms near the time axes. The reflection from the acrylic-orthorhombic interface begins at about 1410 ms. The event beginning at about 1650 ms is likely a PS conversion. Its amplitude at near offsets is very weak, and it has a moveout velocity that is decidedly slower than that of the nearby P-wave reflection. Mahmoudian et al. (2011; this volume) have taken the CMP gathers all 16 azimuths (0º, ±14º, ±27º, ±37º, ±45º, ±57º, ±67º, ±76º, and 90º) and inverted the AVAZ data from the acrylic-phenolic interface to estimate the elastic moduli for the orthorhombic layer.

In this report, AVAZ analysis of the reflections on the physically-modeled data is at a fairly rudimentary level. However, we anticipate that more sophisticated treatment will be applied to these data, as has already begun by Mahmoudian et al. (2011). Similar to AVAZ analysis of real-world field data, the AVAZ analysis of physically-modeled amplitudes can be very challenging, simply because of the fact that the available theoretical models used for analysis cannot account for all the conditions of a real experimental survey. Appendix B gives some guidelines on required corrections and procedures for analyzing and interpreting the modeled AVAZ data. In particular, all observed amplitudes must be corrected for radiation/reception directivities of the piezopin transducers.

FUTURE 3D SURVEYS INVOVING ANISOTROPIC MEDIUM

Solid slab #3 shown on Figure 1c was designed as a target for 3D surveys. Figure 14a shows a side view of the experimental setup for doing such a survey in the near future. We are hoping that the amplitude information will allow us to image the individual pucks. We may be to find robust azimuth-dependent seismic attributes that correlate with the direction of maximum P-wave velocity.

A second experimental setup that is suitable for 3D acquisition is shown on Figure 14b, in which a small cylindrical PVC target is placed beneath an isotropic acrylic layer and the homogeneous or inhomogeneous orthorhombic layer. A marine 3D survey over

this model would produce a dataset suitable for testing techniques for migration and imaging through orthorhombic media. Because of the orthorhombic layer, Kirchoff migration to image the cylindrical target requires ray-tracing using anisotropic velocities.

A possible method for doing this may be the procedure given by Daley (2010) for defining velocities in orthorhombic media and ray-tracing through them. In Appendix A, we present an alternative set of simpler equations for defining qP group velocities in orthorhombic media. The equations are an extension of the Byun et al. (1989) approximation for P-wave velocities in VTI media. Combining these approximate velocities with two-point ray-tracing using Fermat's principle may be an effective way to generate raypaths and arrival times suitable for migrating through the orthorhombic layer.

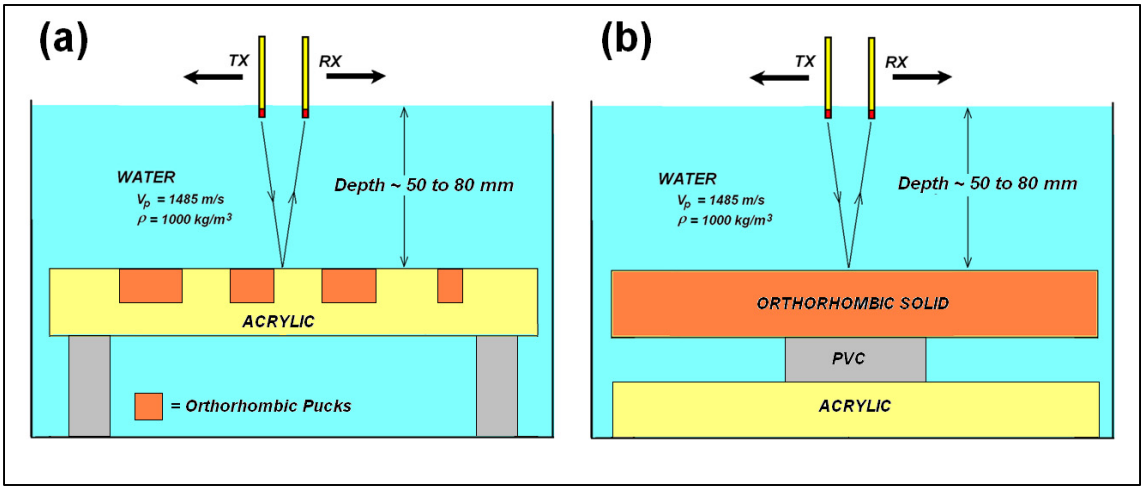

FIG 14. Two possible models as targets for marine 3D surveys to acquire data to test algorithms for imaging media with orthorhombic anisotropy.

SUMMARY AND DISCUSSION

Using sections of orthorhombic phenolic material, we have fabricated slabs of orthorhombic material with P-wave velocities in the x, y, and z axes of 3550 m/s, 2950 m/s, and 3400 m/s, respectively. By immersing one of these slabs in water, we produced a two-layer velocity model. By placing a slab of isotropic acrylic plastic above the orthorhombic slab, we produced a three-layer velocity model. We used the University of Calgary Seismic Physical Modeling facility to record CMP gathers files along many azimuth angles over these models. Picked arrival times and estimated amplitudes from reflections off the orthorhombic layer for these azimuths exhibit VVAZ and AVAZ behavior, confirming the claim that the physically-modeled CMP gathers contain data suitable for VVAZ/AVAZ analysis.

All the physically-modeled data acquired in this project are stored as SEGY files, and they will be available to our sponsors upon request.

ACKNOWLEDGEMENTS

We are grateful to NSERC and the industrial sponsors of CREWES for supporting this research.

REFERENCES

Byun, B.S., Corrigan, D., and Gaider, J.E., 1989. Anisotropic velocity analysis for lithology discrimination, Geophysics, **54**, 1566-1574.

Daley, P.F., 2010. A linearized group velocity approach for two-point qP ray tracing in a layered orthorhombic medium, CREWES Research Report **22**, 17.1-17.15.

Daley, P.F., 2011. Finite difference methods for wave propagation in an elastic anisotropic plane-layered medium with orthorhombic symmetry, CREWES Research Report 23, this volume.

Graebner, M., 1992. Plane-wave reflection and transmission coefficients for transversely isotropic solid, Geophysics, **57**, 1512-1519.

Hasse, A.B., and Ursenbach, C.P., 2005. Spherical-wave AVO modeling in elastic VTI media, CREWES Research Report **17**, 13.1-13.7.

Haase, A.B., 2005. Anelasticity and spherical-wave AVO-modelling in VTI-media, CREWES Research Report 17, 14.1-14.8.

Kumar, D., Sen, M.K., and Ferguson, R.J., 2004. Traveltime calculation and prestack depth migration in tilted transversely isotropic media, Geophysics, **69**, 37-44.

Mahmoudian, F., Margrave, G.F., Daley, P.F., Wong, J., and Gallant, E, 2010. Determining elastic constants of an orthorhombic material by physical seismic modeling, CREWES Research Report **22**, 60.1-60.23.

Mahmoudian, F., Margrave, Wong, J., and Russel, B., 2011. AVAZ inversion for anisotropy parameters of a fractured medium: A physical modeling study, CREWES Research Report **23**, this volume.

Varyčuk, V., and Pšenčik, I., 1998. PP reflection coefficients in weakly anisotropic media, Geophysics, **63**, 2129-2941.

Ursenbach, C.P., Hasse, A.B., Downton, J.E., 2006. Improved modeling of spherical-wave AVO, CREWES Research Report **18**, 27.1-27.25.

Wong, J. and Mahmoudian, F., 2011. Physical modeling II: directivities of disc transducers, CREWES Research Reports 23, this volume.

Wong, J., Hall, K.H., Gallant, E., Maier, R., Bertram, M., and Lawton, D.C., 2009. Seismic physical modeling at the University of Calgary, CSEG Recorder, **34**, 36-43.

APPENDIX A: GUIDELINES FOR VVAZ ANALYSIS

The phenolic slab is a medium with orthorhombic anisotropy that has different V_p and V_s values along the principal axes. In order to do proper VVAZ analysis of the physically-modeled data described in this report, we must have mathematical procedures or expressions that describe angle-dependence of velocities in a media with orthorhombic anisotropy.

Daley (2010) has implemented a procedure for determining V_p and V_s values in an orthorhombic medium as a function of the polar angle θ and the azimuthal angle φ, and for ray-tracing through such a medium. The procedure uses the elastic constants $C_{i,j}$ as input and calculates velocities $V_p(\varphi, \theta)$ and $V_s(\varphi, \theta)$.

An alternative, simplified treatment of the P-wave velocities in orthorhombic media may be useful for initial analysis of the VVAZ behaviour observed in the physically modeled data. We extend the Byun approximation to describe the P-wave group velocities $V_p(\varphi, \theta)$ in an orthorhombic medium. Byun et al. (1989) published the following formulas that approximate VTI group velocities for P waves:

$$V_p^{-2}(\theta) = a_0 + a_1 \cos^2\theta - a_2 \cos^4\theta \ , \quad \text{(A1)}$$

$$a_0 = V_h^{-2} \ , \quad \text{(A2)}$$

$$a_1 = 4V_{45}^{-2} - 3V_h^{-2} - V_v^{-2} \ , \quad \text{(A3)}$$

$$a_2 = 4V_{45}^{-2} - 2V_h^{-2} - 2V_v^{-2} \ , \quad \text{(A4)}$$

where V_v, V_h, and V_{45} are the group velocities in the vertical (θ=0°), horizontal (θ=90°), and 45° dip angle directions. For the isotropic case, a_1 and a_2 are identically zero.

In the orthorhombic case, the velocities V_h, and V_{45} vary with the azimuth angle φ. We can approximate this variation by a form similar to that of Equations A1 to A4:

$$v_p^{-2}(\varphi) = b_0 + b_1 \cos^2\varphi - b_2 \cos^4\varphi \ , \quad \text{(A5)}$$

$$b_0 = v_x^{-2} \ , \quad \text{(A6)}$$

$$b_1 = 4v_{45}^{-2} - 3v_x^{-2} - v_y^{-2} \ , \quad \text{(A7)}$$

$$b_2 = 4v_{45}^{-2} - 2v_x^{-2} - 2v_y^{-2} \ , \quad \text{(A8)}$$

where v_x, v_y, and v_{45} are the group velocities along the x-axis (φ=0°), along the y-axis (φ=90°), and along the φ=45° azimuth direction. For the isotropic case, b_1 and b_2 are identically zero. Combining Equations A5-A8 with Equations A1-A4 yields the following approximation for P-wave group velocities $c_p(\varphi, \theta)$ in orthorhombic media:

$$c_p^{-2}(\varphi, \theta) = c_0 + c_1 \cos^2\theta - c_2 \cos^4\theta \ , \quad \text{(A9)}$$

$$c_0(\varphi) = v_p^{-2}(\varphi) \ , \quad \text{(A10)}$$

$$c_1(\varphi) = 4V_{45}^{-2}(\varphi) - 3v_p^{-2}(\varphi) - V_v^{-2} \ , \quad \text{(A11)}$$

$$c_2(\varphi) = 4V_{45}^{-2}(\varphi) - 2v_p^{-2}(\varphi) - 2V_v^{-2} \ . \quad \text{(A12)}$$

We emphasize that φ is measured from the horizontal x-axis and θ is measured from the vertical z-axis. For all φ and θ, the values of V_v, v_x, v_y, and v_{45} are assumed to be constant for a given orthorhombic medium. For a given azimuth φ, the value of $V_{45}(\varphi)$ must be chosen to fit velocities and/or first arrival times observed in the vertical plane with azimuth φ.

The above approximate velocities for orthorhombic media can used to do two-point ray tracing based on Fermat's principle. The suitability of applying this method to fit measured data is yet untested.

APPENDIX B: AVAZ ANALYIS

For spherical waves, we currently do not have software that enables us to calculate reflection amplitudes from interfaces involving orthorhombic media. The spherical-wave Zoeppritz Explorer (Ursenbach et al.; 2006) available from the CREWES website enables us to calculate spherical-wave reflections coefficients involving only isotropic media, and the current form of the VTI Explorer, based on equations published by Graebner (1992), addresses plane waves and not spherical waves. Hasse and Ursenbach (2005) have extended Graebner's equations to account for the effects of spherical waves, but to date their equations have not been coded. Rüger (1992) and Pšenčik et al. (2001) presented linearized coefficients for plane wave reflections off interfaces between HTI and orthorhombic media.

In the absence of a compact set of equations that given a reasonably accurate description of reflection amplitudes from interfaces between orthorhombic media, we resort to the following in order to do at least a preliminary AVAZ analysis of the physically-modeled data:

1. At each azimuth, we can compare the observed AVO effect with calculations from the spherical-wave, isotropic media model.

2. At each azimuth, we can compare the observed AVO effect with calculations from the plane-wave, VTI media model.

Directivity Corrections for measured Amplitudes

Disc-shaped transducers used to generate and detect vibrational signals in an acoustic medium such as water have pronounced directional radiation and reception patterns. Their diameters are in practice significant fractions of the radiated wavelengths, and therefore significant wave interference effects will occur. Constructive and destructive interference causes the amplitudes of transmitted and received signals to have a strong angular dependence or directivity in the planes containing the disc axes. Before AVO/AVAZ analysis can be done on measured signal amplitudes, corrections must be made for the directivity.

Directivities of disc-shaped piezoelectric transducers operating in an acoustic medium have been calculated numerically and analytically (Wong and Mahmoudian, 2011; this volume). The combined directivity (amplitude variation with polar angle θ) of a pair of disc-shaped transducers used as a source and a receiver is

$$F(\theta) = [(z/R) * U_r^N]^2 \sim [\cos\theta * J_1(X)/X]^2 \ , \qquad \text{(B1)}$$

$$X = (\pi D \sin\theta)/\lambda = (\pi D \sin\theta) * (f/c) \ . \qquad \text{(B2)}$$

$J_1(X)$ is the Bessel function of order 1. The controlling parameter for these equations is the ratio of disc diameter D to wavelength. The directivities given by Equations B1 and B2 have been used to correct the reflection amplitudes measured from a water-acrylic interface on a physical model. The correction is approximate since Equations B1 and B2 are for a single frequency, whereas a seismic wavelet consists of a range of frequencies (for measured data, f is set to the dominant frequency of the observed wavelets).

On Figure B1, the corrected amplitudes for the reflection off a water-acrylic interface are compared to the isotropic AVO responses predicted by the Zoeppritz equations and by the spherical wave reflectivity analysis of Ursenbach et al. (2006). While the AVO response from the physical model conforms closely to the Zoeppritz predictions for angle about 10 degrees less than the critical angle (indicated by the short blue line on the horizontal axis at 32.8º), it is in good agreement with the spherical wave reflectivity predictions for angles up to and slightly beyond the critical angle.

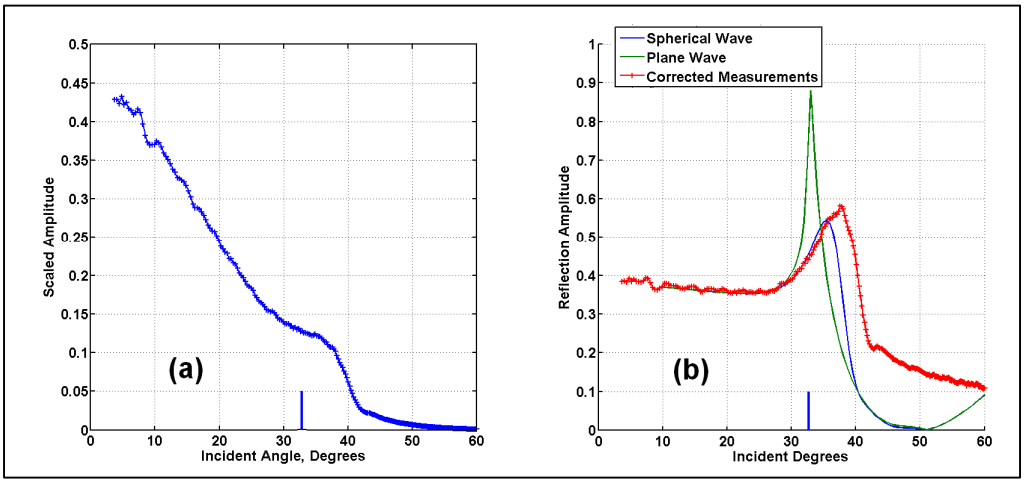

FIG. B1. (a) Observed reflection amplitudes from a water-acrylic interface versus incident angle. (b) Corrected amplitudes compared to theoretically-predicted AVA behaviour.

Verifying azimuthal isotropy of measurement system

An important consideration in using physically modeled data for AVAZ analysis is that the measurement system itself possesses no anisotropy. We tested for this condition by making NMO velocity and amplitude measurements on reflections off water-acrylic interfaces. Since both water and acrylic are isotropic materials, neither the NMO velocities nor the reflection amplitudes should exhibit any azimuth dependence.

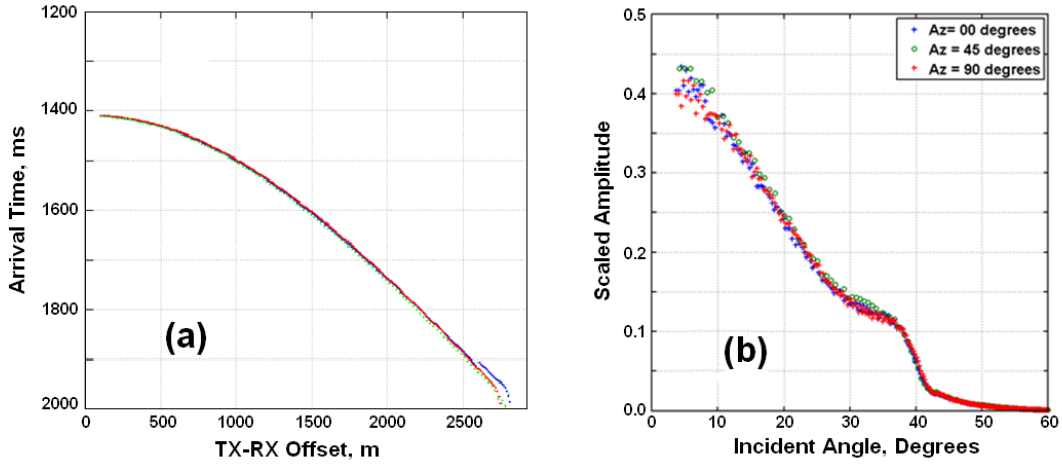

FIG. B2. (a) Two-way reflection times through water and an isotropic acrylic layer for three azimuths. (b) Observed peak-to trough amplitudes for reflections off a water-acrylic interface.

Measured arrival times and AVO amplitudes of reflections off water-acrylic interfaces for a number of azimuth directions showed little or no variation with azimuth. Figure B2a shows the measured arrival times for reflection times from the water-acrylic interface for three azimuths (0º, 45º, 90º). Figure B2b shows the measured AVO response from the water-acrylic interface for the same three azimuths (0º, 45º, 90º). The figures verify that the measurement system of the modeling facility gives isotropic results in media that are azimuthally isotropic.

APPENDIX C: PIEZOPIN WAVELETS

Figure C1 shows two piezopins mounted on the positioning system with their active tips extending slightly below the water surface by the same distance. The figure shows three paths that the signal takes to go front the tip of the transmitting piezopin TX to the tip of the receiving piezopin RX. We recorded seismograms as the tip depths z increase of both transducers by two meter increments the TX-RX lateral separation fixed at 100 m. Figure C2 shows the waveforms of the arrivals associated with the primary reflection from a water-solid interface at a depth of about 700 m. The waveforms depend on how far the active tips extend below the surface. The reflected event splits up into three distinct arrivals as tip depths increase from 0 m to 100 m.

The earliest arrival A follows the path from the TX tip down to the reflecting interface and up to the RX (Figure C1a). Its time of arrival decreases as tip depths increase since both tips move closer to the reflecting interface as tip depths increase.

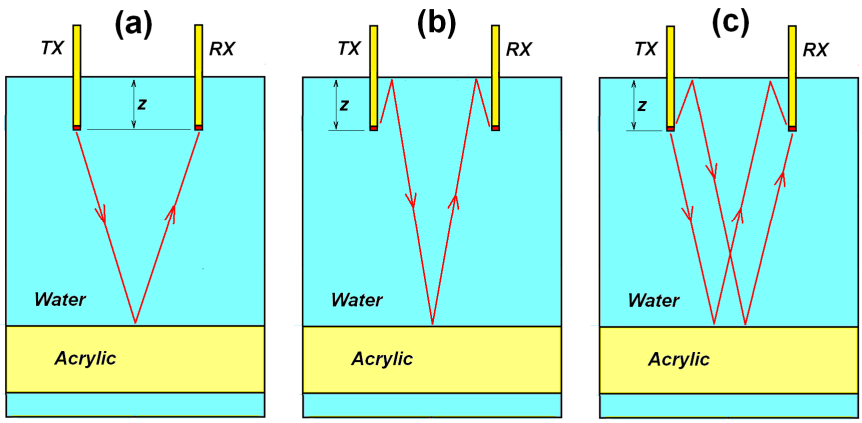

FIG. C1. Three travel paths taken by an acoustic signal from the tip of a transmitting transducer TX to the tip of a receiving transducer RX.

The latest arrival B is a ghost. It travels along the path from the TX tip up to the water surface, down to the reflecting interface, up again to the water surface, and finally down to the RX tip (Figure C1b). The time of arrival for this event increases with tip depths since the total travel path length increases with tip depth.

The middle event C has arrival times with little if any moveout with changes in tip depths. The associated path lengths must change very little as tip depths change. Figure C1c shows a double ghost with paths that meets this condition. One of the paths on

Figure C1c goes down from the transmitting transducer tip to the reflector, then up to the water surface, and finally down to the receiving transducer tip. The second path for the double ghost also shows a single bounce off the water surface.

The waveforms on Figure C2 are plotted with constant gain, so the trace-to-trace relative amplitudes of the arrivals are true. The amplitude of arrival A stays constant over the range of the tip depths shown, while the other two arrival show more complex behaviour, possibly indicating complex interaction between the transducer bodies and the water surface. The double ghost C appears to be stronger than arrivals A and B.

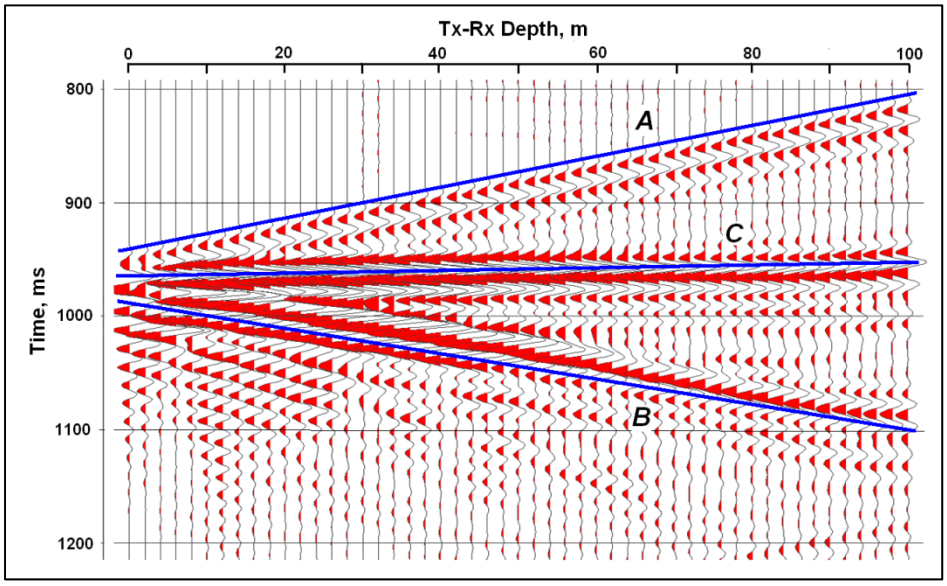

FIG. C2. Reflected waveforms as a function of tip depth z. The reflection from the water-acrylic boundary splits up into three distinct arrivals A, B, and C as z increases.

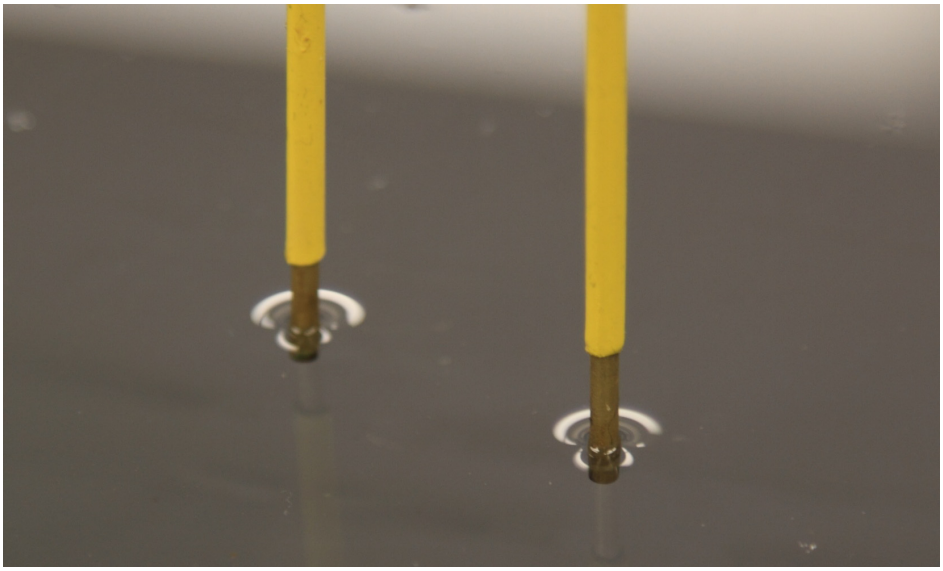

FIG. C3. Photograph showing the menisci around two piezopins. The diameters of the menisci can be estimated to be in the range 4 to 7 mm, based on the fact that the diameters of the piezopin tips are 2.36 mm.

From Figure C2, we see that the wavelet shapes change with depth changes of 2 m (world scale) or 0.2 mm (model scale). In conducting marine-type surveys, we try to set the tips at exactly the same height above or below the water surface. The repeatability of this equal-height setting is difficult to achieve within 0.1 mm. We also try to keep the reflected wavelet at compact as possible. From the traces on Figure C2, that means we must use the smallest tip depths possible. In fact, we have found that the most compact reflected wavelets result when the tip depths are almost a millimeter above the global water surface. In this case, the tips still is in contact with the water because adhesion forces lifts the water surface like a membrane and causes a meniscus to form around each tip. Figure C3 shows the menisci around two piezopins. When the piezopin tips are close to the surface, the wavelet shapes are influenced by complex, unspecified interactions between the disc transducers and the curved shape of the water menisci.

APPENDIX D: KEEPING CONSTANT WATER LEVEL

A high-resolution marine 3D survey may involve continuous recording over a period of several days. Inevitably, evaporation of water will take place. Without intervention, the tips of the piezopin transducers will gradually lose contact with the water, and no signals will be recorded. Also, if evaporation decreases the distance between the active tips and the surface of the water, the recorded wavelets will change, as was shown in Appendix C. It is thus important to have a means of compensating for evaporation and keeping the water level as constant as possible. Figure D1 shows a workable fill-and-spill technique for achieving this.

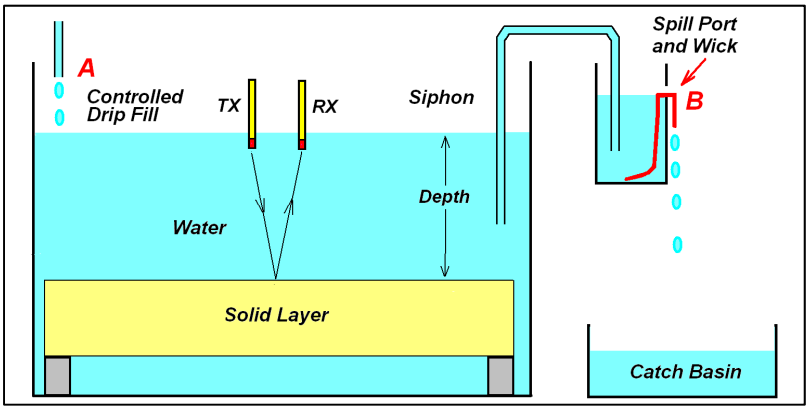

FIG. D1. An arrangement for counteracting evaporation loss and maintaining a constant water level in the modeling tank.

At point A, water slowly drips into the modeling tank which is linked by a water-filled siphon to an external spill container with an outlet port B. The height of the spill container and its port is adjustable. Because of the link through the siphon, the water levels in the modeling tank and the spill container must be the same. If the levels are below the spill port, they will rise due to the drip fill. Once the levels rise to the level of the spill port, water will spill out. Slow spilling through the port is assisted by the capillary action of a wick. The evaporation loss and the spill rate will match the fill rate, so the water levels will stay constant at the level of the spill port. This short-term, primitive solution will be replaced by design that adds water to the tank through a valve that open and closes automatically according to an electronically-sensed water level.